

Measurement of the branching fraction of the singly Cabibbo-suppressed decay $\Lambda_c^+ \rightarrow \Lambda K^+$

M. Ablikim,¹ M. N. Achasov,^{11,b} P. Adlarson,⁷⁰ M. Albrecht,⁴ R. Aliberti,³¹ A. Amoroso,^{69a,69c} M. R. An,³⁵ Q. An,^{66,53} X. H. Bai,⁶¹ Y. Bai,⁵² O. Bakina,³² R. Baldini Ferroli,^{26a} I. Balossino,^{27a} Y. Ban,^{42,g} S. S. Bao,⁴⁵ V. Batozskaya,^{1,40} D. Becker,³¹ K. Begzsuren,²⁹ N. Berger,³¹ M. Bertani,^{26a} D. Bettoni,^{27a} F. Bianchi,^{69a,69c} J. Bloms,⁶³ A. Bortone,^{69a,69c} I. Boyko,³² R. A. Briere,⁵ A. Brueggemann,⁶³ H. Cai,⁷¹ X. Cai,^{1,53} A. Calcaterra,^{26a} G. F. Cao,^{1,58} N. Cao,^{1,58} S. A. Cetin,^{57a} J. F. Chang,^{1,53} W. L. Chang,^{1,58} G. Chelkov,^{32,a} C. Chen,³⁹ Chao Chen,⁵⁰ G. Chen,¹ H. S. Chen,^{1,58} M. L. Chen,^{1,53} S. J. Chen,³⁸ S. M. Chen,⁵⁶ T. Chen,¹ X. R. Chen,^{28,58} X. T. Chen,¹ Y. B. Chen,^{1,53} Z. J. Chen,^{23,h} W. S. Cheng,^{69c} S. K. Choi,⁵⁰ X. Chu,³⁹ G. Cibinetto,^{27a} F. Cossio,^{69c} J. J. Cui,⁴⁵ H. L. Dai,^{1,53} J. P. Dai,⁷³ A. Dbeyssi,¹⁷ R. E. de Boer,⁴ D. Dedovich,³² Z. Y. Deng,¹ A. Denig,³¹ I. Denysenko,³² M. Destefanis,^{69a,69c} F. De Mori,^{69a,69c} Y. Ding,³⁶ J. Dong,^{1,53} L. Y. Dong,^{1,58} M. Y. Dong,^{1,53,58} X. Dong,⁷¹ S. X. Du,⁷⁵ P. Egorov,^{32,a} Y. L. Fan,⁷¹ J. Fang,^{1,53} S. S. Fang,^{1,58} W. X. Fang,¹ Y. Fang,¹ R. Farinelli,^{27a} L. Fava,^{69b,69c} F. Feldbauer,⁴ G. Felici,^{26a} C. Q. Feng,^{66,53} J. H. Feng,⁵⁴ K. Fischer,⁶⁴ M. Fritsch,⁴ C. Fritzscht,⁶³ C. D. Fu,¹ H. Gao,⁵⁸ Y. N. Gao,^{42,g} Yang Gao,^{66,53} S. Garbolino,^{69c} I. Garzia,^{27a,27b} P. T. Ge,⁷¹ Z. W. Ge,³⁸ C. Geng,⁵⁴ E. M. Gersabeck,⁶² A. Gilman,⁶⁴ K. Goetzen,¹² L. Gong,³⁶ W. X. Gong,^{1,53} W. Gradl,³¹ M. Greco,^{69a,69c} L. M. Gu,³⁸ M. H. Gu,^{1,53} Y. T. Gu,¹⁴ C. Y. Guan,^{1,58} A. Q. Guo,^{28,58} L. B. Guo,³⁷ R. P. Guo,⁴⁴ Y. P. Guo,^{10,f} A. Guskov,^{32,a} T. T. Han,⁴⁵ W. Y. Han,³⁵ X. Q. Hao,¹⁸ F. A. Harris,⁶⁰ K. K. He,⁵⁰ K. L. He,^{1,58} F. H. Heinsius,⁴ C. H. Heinz,³¹ Y. K. Heng,^{1,53,58} C. Herold,⁵⁵ M. Himmelreich,^{31,d} G. Y. Hou,^{1,58} Y. R. Hou,⁵⁸ Z. L. Hou,¹ H. M. Hu,^{1,58} J. F. Hu,^{51,i} T. Hu,^{1,53,58} Y. Hu,¹ G. S. Huang,^{66,53} K. X. Huang,⁵⁴ L. Q. Huang,^{28,58} X. T. Huang,⁴⁵ Y. P. Huang,¹ Z. Huang,^{42,g} T. Hussain,⁶⁸ N. Hüsken,^{25,31} W. Imoehl,²⁵ M. Irshad,^{66,53} J. Jackson,²⁵ S. Jaeger,⁴ S. Janchiv,²⁹ E. Jang,⁵⁰ J. H. Jeong,⁵⁰ Q. Ji,¹ Q. P. Ji,¹⁸ X. B. Ji,^{1,58} X. L. Ji,^{1,53} Y. Y. Ji,⁴⁵ Z. K. Jia,^{66,53} H. B. Jiang,⁴⁵ S. S. Jiang,³⁵ X. S. Jiang,^{1,53,58} Y. Jiang,⁵⁸ J. B. Jiao,⁴⁵ Z. Jiao,²¹ S. Jin,³⁸ Y. Jin,⁶¹ M. Q. Jing,^{1,58} T. Johansson,⁷⁰ N. Kalantar-Nayestanaki,⁵⁹ X. S. Kang,³⁶ R. Kappert,⁵⁹ B. C. Ke,⁷⁵ I. K. Keshk,⁴ A. Khoukaz,⁶³ R. Kiuchi,¹ R. Kliemt,¹² L. Koch,³³ O. B. Kolcu,^{57a} B. Kopf,⁴ M. Kuemmel,⁴ M. Kuessner,⁴ A. Kupsc,^{40,70} W. Kühn,³³ J. J. Lane,⁶² J. S. Lange,³³ P. Larin,¹⁷ A. Lavania,²⁴ L. Lavezzi,^{69a,69c} Z. H. Lei,^{66,53} H. Leithoff,³¹ M. Lellmann,³¹ T. Lenz,³¹ C. Li,⁴³ C. Li,³⁹ C. H. Li,³⁵ Cheng Li,^{66,53} D. M. Li,⁷⁵ F. Li,^{1,53} G. Li,¹ H. Li,⁴⁷ H. Li,^{66,53} H. B. Li,^{1,58} H. J. Li,¹⁸ H. N. Li,^{51,i} J. Q. Li,⁴ J. S. Li,⁵⁴ J. W. Li,⁴⁵ Ke Li,¹ L. J. Li,¹ L. K. Li,¹ Lei Li,³ M. H. Li,³⁹ P. R. Li,^{34,j,k} S. X. Li,¹⁰ S. Y. Li,⁵⁶ T. Li,⁴⁵ W. D. Li,^{1,58} W. G. Li,¹ X. H. Li,^{66,53} X. L. Li,⁴⁵ Xiaoyu Li,^{1,58} Z. X. Li,¹⁴ H. Liang,^{66,53} H. Liang,^{1,58} H. Liang,³⁰ Y. F. Liang,⁴⁹ Y. T. Liang,^{28,58} G. R. Liao,¹³ L. Z. Liao,⁴⁵ J. Libby,²⁴ A. Limphirat,⁵⁵ C. X. Lin,⁵⁴ D. X. Lin,^{28,58} T. Lin,¹ B. J. Liu,¹ C. X. Liu,¹ D. Liu,^{17,66} F. H. Liu,⁴⁸ Fang Liu,¹ Feng Liu,⁶ G. M. Liu,^{51,i} H. Liu,^{34,j,k} H. B. Liu,¹⁴ H. M. Liu,^{1,58} Huanhuan Liu,¹ Huihui Liu,¹⁹ J. B. Liu,^{66,53} J. L. Liu,⁶⁷ J. Y. Liu,^{1,58} K. Liu,¹ K. Y. Liu,³⁶ Ke Liu,²⁰ L. Liu,^{66,53} Lu Liu,³⁹ M. H. Liu,^{10,f} P. L. Liu,¹ Q. Liu,⁵⁸ S. B. Liu,^{66,53} T. Liu,^{10,f} W. K. Liu,³⁹ W. M. Liu,^{66,53} X. Liu,^{34,j,k} Y. Liu,^{34,j,k} Y. B. Liu,³⁹ Z. A. Liu,^{1,53,58} Z. Q. Liu,⁴⁵ X. C. Lou,^{1,53,58} F. X. Lu,⁵⁴ H. J. Lu,²¹ J. G. Lu,^{1,53} X. L. Lu,¹ Y. Lu,⁷ Y. P. Lu,^{1,53} Z. H. Lu,¹ C. L. Luo,³⁷ M. X. Luo,⁷⁴ T. Luo,^{10,f} X. L. Luo,^{1,53} X. R. Lyu,⁵⁸ Y. F. Lyu,³⁹ F. C. Ma,³⁶ H. L. Ma,¹ L. L. Ma,⁴⁵ M. M. Ma,^{1,58} Q. M. Ma,¹ R. Q. Ma,^{1,58} R. T. Ma,⁵⁸ X. Y. Ma,^{1,53} Y. Ma,^{42,g} F. E. Maas,¹⁷ M. Maggiora,^{69a,69c} S. Maldaner,⁴ S. Malde,⁶⁴ Q. A. Malik,⁶⁸ A. Mangoni,^{26b} Y. J. Mao,^{42,g} Z. P. Mao,¹ S. Marcello,^{69a,69c} Z. X. Meng,⁶¹ G. Mezzadri,^{27a} H. Miao,¹ T. J. Min,³⁸ R. E. Mitchell,²⁵ X. H. Mo,^{1,53,58} N. Yu. Muchnoi,^{11,b} Y. Nefedov,³² F. Nerling,^{17,d} I. B. Nikolaev,^{11,b} Z. Ning,^{1,53} S. Nisar,⁹¹ Y. Niu,⁴⁵ S. L. Olsen,⁵⁸ Q. Ouyang,^{1,53,58} S. Pacetti,^{26b,26c} X. Pan,^{10,f} Y. Pan,⁵² A. Pathak,³⁰ M. Pelizaeus,⁴ H. P. Peng,^{66,53} K. Peters,^{12,d} J. L. Ping,³⁷ R. G. Ping,^{1,58} S. Plura,³¹ S. Pogodin,³² V. Prasad,^{66,53} F. Z. Qi,¹ H. Qi,^{66,53} H. R. Qi,⁵⁶ M. Qi,³⁸ T. Y. Qi,^{10,f} S. Qian,^{1,53} W. B. Qian,⁵⁸ Z. Qian,⁵⁴ C. F. Qiao,⁵⁸ J. J. Qin,⁶⁷ L. Q. Qin,¹³ X. P. Qin,^{10,f} X. S. Qin,⁴⁵ Z. H. Qin,^{1,53} J. F. Qiu,¹ S. Q. Qu,⁵⁶ K. H. Rashid,⁶⁸ C. F. Redmer,³¹ K. J. Ren,³⁵ A. Rivetti,^{69c} V. Rodin,⁵⁹ M. Rolo,^{69c} G. Rong,^{1,58} Ch. Rosner,¹⁷ S. N. Ruan,³⁹ H. S. Sang,⁶⁶ A. Sarantsev,^{32,c} Y. Schelhaas,³¹ C. Schnier,⁴ K. Schoenning,⁷⁰ M. Scodreggio,^{27a,27b} K. Y. Shan,^{10,f} W. Shan,²² X. Y. Shan,^{66,53} J. F. Shangguan,⁵⁰ L. G. Shao,^{1,58} M. Shao,^{66,53} C. P. Shen,^{10,f} H. F. Shen,^{1,58} X. Y. Shen,^{1,58} B. A. Shi,⁵⁸ H. C. Shi,^{66,53} J. Y. Shi,¹ q. q. Shi,⁵⁰ R. S. Shi,^{1,58} X. Shi,^{1,53} X. D. Shi,^{66,53} J. J. Song,¹⁸ W. M. Song,^{30,1} Y. X. Song,^{42,g} S. Sosio,^{69a,69c} S. Spataro,^{69a,69c} F. Stieler,³¹ K. X. Su,⁷¹ P. P. Su,⁵⁰ Y. J. Su,⁵⁸ G. X. Sun,¹ H. Sun,⁵⁸ H. K. Sun,¹ J. F. Sun,¹⁸ L. Sun,⁷¹ S. S. Sun,^{1,58} T. Sun,^{1,58} W. Y. Sun,³⁰ X. Sun,^{23,h} Y. J. Sun,^{66,53} Y. Z. Sun,¹ Z. T. Sun,⁴⁵ Y. H. Tan,⁷¹ Y. X. Tan,^{66,53} C. J. Tang,⁴⁹ G. Y. Tang,¹ J. Tang,⁵⁴ L. Y. Tao,⁶⁷ Q. T. Tao,^{23,h} M. Tat,⁶⁴ J. X. Teng,^{66,53} V. Thoren,⁷⁰ W. H. Tian,⁴⁷ Y. Tian,^{28,58} I. Uman,^{57b} B. Wang,¹ B. L. Wang,⁵⁸ C. W. Wang,³⁸ D. Y. Wang,^{42,g} F. Wang,⁶⁷ H. J. Wang,^{34,j,k} H. P. Wang,^{1,58} K. Wang,^{1,53} L. L. Wang,¹ M. Wang,⁴⁵ M. Z. Wang,^{42,g} Meng Wang,^{1,58} S. Wang,¹³ S. Wang,^{10,f} T. Wang,^{10,f} T. J. Wang,³⁹ W. Wang,⁵⁴ W. H. Wang,⁷¹ W. P. Wang,^{66,53} X. Wang,^{42,g} X. F. Wang,^{34,j,k} X. L. Wang,^{10,f} Y. Wang,⁵⁶ Y. D. Wang,⁴¹ Y. F. Wang,^{1,53,58} Y. H. Wang,⁴³ Y. Q. Wang,¹ Yaqian Wang,^{16,1} Z. Wang,^{1,53} Z. Y. Wang,^{1,58} Ziyi Wang,⁵⁸ D. H. Wei,¹³ F. Weidner,⁶³ S. P. Wen,¹ D. J. White,⁶² U. Wiedner,⁴ G. Wilkinson,⁶⁴ M. Wolke,⁷⁰ L. Wollenberg,⁴ J. F. Wu,^{1,58} L. H. Wu,¹ L. J. Wu,^{1,58} X. Wu,^{10,f} X. H. Wu,³⁰ Y. Wu,⁶⁶ Z. Wu,^{1,53} L. Xia,^{66,53} T. Xiang,^{42,g} D. Xiao,^{34,j,k} G. Y. Xiao,³⁸ H. Xiao,^{10,f}

S. Y. Xiao,¹ Y. L. Xiao,^{10,f} Z. J. Xiao,³⁷ C. Xie,³⁸ X. H. Xie,^{42,g} Y. Xie,⁴⁵ Y. G. Xie,^{1,53} Y. H. Xie,⁶ Z. P. Xie,^{66,53} T. Y. Xing,^{1,58} C. F. Xu,¹ C. J. Xu,⁵⁴ G. F. Xu,¹ H. Y. Xu,⁶¹ Q. J. Xu,¹⁵ X. P. Xu,⁵⁰ Y. C. Xu,⁵⁸ Z. P. Xu,³⁸ F. Yan,^{10,f} L. Yan,^{10,f} W. B. Yan,^{66,53} W. C. Yan,⁷⁵ H. J. Yang,^{46,e} H. L. Yang,³⁰ H. X. Yang,¹ L. Yang,⁴⁷ S. L. Yang,⁵⁸ Tao Yang,¹ Y. F. Yang,³⁹ Y. X. Yang,^{1,58} Yifan Yang,^{1,58} M. Ye,^{1,53} M. H. Ye,⁸ J. H. Yin,¹ Z. Y. You,⁵⁴ B. X. Yu,^{1,53,58} C. X. Yu,³⁹ G. Yu,^{1,58} T. Yu,⁶⁷ X. D. Yu,^{42,g} C. Z. Yuan,^{1,58} L. Yuan,² S. C. Yuan,¹ X. Q. Yuan,¹ Y. Yuan,^{1,58} Z. Y. Yuan,⁵⁴ C. X. Yue,³⁵ A. A. Zafar,⁶⁸ F. R. Zeng,⁴⁵ X. Zeng,⁶ Y. Zeng,^{23,h} Y. H. Zhan,⁵⁴ A. Q. Zhang,¹ B. L. Zhang,¹ B. X. Zhang,¹ D. H. Zhang,³⁹ G. Y. Zhang,¹⁸ H. Zhang,⁶⁶ H. H. Zhang,³⁰ H. H. Zhang,⁵⁴ H. Y. Zhang,^{1,53} J. L. Zhang,⁷² J. Q. Zhang,³⁷ J. W. Zhang,^{1,53,58} J. X. Zhang,^{34,j,k} J. Y. Zhang,¹ J. Z. Zhang,^{1,58} Jianyu Zhang,^{1,58} Jiawei Zhang,^{1,58} L. M. Zhang,⁵⁶ L. Q. Zhang,⁵⁴ Lei Zhang,³⁸ P. Zhang,¹ Q. Y. Zhang,^{35,75} Shuihan Zhang,^{1,58} Shulei Zhang,^{23,h} X. D. Zhang,⁴¹ X. M. Zhang,¹ X. Y. Zhang,⁴⁵ X. Y. Zhang,⁵⁰ Y. Zhang,⁶⁴ Y. T. Zhang,⁷⁵ Y. H. Zhang,^{1,53} Yan Zhang,^{66,53} Yao Zhang,¹ Z. H. Zhang,¹ Z. Y. Zhang,⁷¹ Z. Y. Zhang,³⁹ G. Zhao,¹ J. Zhao,³⁵ J. Y. Zhao,^{1,58} J. Z. Zhao,^{1,53} Lei Zhao,^{66,53} Ling Zhao,¹ M. G. Zhao,³⁹ Q. Zhao,¹ S. J. Zhao,⁷⁵ Y. B. Zhao,^{1,53} Y. X. Zhao,^{28,58} Z. G. Zhao,^{66,53} A. Zhemchugov,^{32,a} B. Zheng,⁶⁷ J. P. Zheng,^{1,53} Y. H. Zheng,⁵⁸ B. Zhong,³⁷ C. Zhong,⁶⁷ X. Zhong,⁵⁴ H. Zhou,⁴⁵ L. P. Zhou,^{1,58} X. Zhou,⁷¹ X. K. Zhou,⁵⁸ X. R. Zhou,^{66,53} X. Y. Zhou,³⁵ Y. Z. Zhou,^{10,f} J. Zhu,³⁹ K. Zhu,¹ K. J. Zhu,^{1,53,58} L. X. Zhu,⁵⁸ S. H. Zhu,⁶⁵ S. Q. Zhu,³⁸ T. J. Zhu,⁷² W. J. Zhu,^{10,f} Y. C. Zhu,^{66,53} Z. A. Zhu,^{1,58} B. S. Zou,¹ and J. H. Zou¹

(BESIII Collaboration)

¹*Institute of High Energy Physics, Beijing 100049, People's Republic of China*²*Beihang University, Beijing 100191, People's Republic of China*³*Beijing Institute of Petrochemical Technology, Beijing 102617, People's Republic of China*⁴*Bochum Ruhr-University, D-44780 Bochum, Germany*⁵*Carnegie Mellon University, Pittsburgh, Pennsylvania 15213, USA*⁶*Central China Normal University, Wuhan 430079, People's Republic of China*⁷*Central South University, Changsha 410083, People's Republic of China*⁸*China Center of Advanced Science and Technology, Beijing 100190, People's Republic of China*⁹*COMSATS University Islamabad, Lahore Campus, Defence Road, Off Raiwind Road, 54000 Lahore, Pakistan*¹⁰*Fudan University, Shanghai 200433, People's Republic of China*¹¹*G.I. Budker Institute of Nuclear Physics SB RAS (BINP), Novosibirsk 630090, Russia*¹²*GSI Helmholtzcentre for Heavy Ion Research GmbH, D-64291 Darmstadt, Germany*¹³*Guangxi Normal University, Guilin 541004, People's Republic of China*¹⁴*Guangxi University, Nanning 530004, People's Republic of China*¹⁵*Hangzhou Normal University, Hangzhou 310036, People's Republic of China*¹⁶*Hebei University, Baoding 071002, People's Republic of China*¹⁷*Helmholtz Institute Mainz, Staudinger Weg 18, D-55099 Mainz, Germany*¹⁸*Henan Normal University, Xinxiang 453007, People's Republic of China*¹⁹*Henan University of Science and Technology, Luoyang 471003, People's Republic of China*²⁰*Henan University of Technology, Zhengzhou 450001, People's Republic of China*²¹*Huangshan College, Huangshan 245000, People's Republic of China*²²*Hunan Normal University, Changsha 410081, People's Republic of China*²³*Hunan University, Changsha 410082, People's Republic of China*²⁴*Indian Institute of Technology Madras, Chennai 600036, India*²⁵*Indiana University, Bloomington, Indiana 47405, USA*^{26a}*INFN Laboratori Nazionali di Frascati, I-00044 Frascati, Italy*^{26b}*INFN Sezione di Perugia, I-06100 Perugia, Italy*^{26c}*University of Perugia, I-06100 Perugia, Italy*^{27a}*INFN Sezione di Ferrara, I-44122 Ferrara, Italy*^{27b}*University of Ferrara, I-44122 Ferrara, Italy*²⁸*Institute of Modern Physics, Lanzhou 730000, People's Republic of China*²⁹*Institute of Physics and Technology, Peace Avenue 54B, Ulaanbaatar 13330, Mongolia*³⁰*Jilin University, Changchun 130012, People's Republic of China*³¹*Johannes Gutenberg University of Mainz, Johann-Joachim-Becher-Weg 45, D-55099 Mainz, Germany*³²*Joint Institute for Nuclear Research, 141980 Dubna, Moscow region, Russia*³³*Justus-Liebig-Universitaet Giessen, II. Physikalisches Institut, Heinrich-Buff-Ring 16, D-35392 Giessen, Germany*³⁴*Lanzhou University, Lanzhou 730000, People's Republic of China*³⁵*Liaoning Normal University, Dalian 116029, People's Republic of China*

- ³⁶Liaoning University, Shenyang 110036, People's Republic of China
³⁷Nanjing Normal University, Nanjing 210023, People's Republic of China
³⁸Nanjing University, Nanjing 210093, People's Republic of China
³⁹Nankai University, Tianjin 300071, People's Republic of China
⁴⁰National Centre for Nuclear Research, Warsaw 02-093, Poland
⁴¹North China Electric Power University, Beijing 102206, People's Republic of China
⁴²Peking University, Beijing 100871, People's Republic of China
⁴³Qufu Normal University, Qufu 273165, People's Republic of China
⁴⁴Shandong Normal University, Jinan 250014, People's Republic of China
⁴⁵Shandong University, Jinan 250100, People's Republic of China
⁴⁶Shanghai Jiao Tong University, Shanghai 200240, People's Republic of China
⁴⁷Shanxi Normal University, Linfen 041004, People's Republic of China
⁴⁸Shanxi University, Taiyuan 030006, People's Republic of China
⁴⁹Sichuan University, Chengdu 610064, People's Republic of China
⁵⁰Soochow University, Suzhou 215006, People's Republic of China
⁵¹South China Normal University, Guangzhou 510006, People's Republic of China
⁵²Southeast University, Nanjing 211100, People's Republic of China
⁵³State Key Laboratory of Particle Detection and Electronics, Beijing 100049, Hefei 230026, People's Republic of China
⁵⁴Sun Yat-Sen University, Guangzhou 510275, People's Republic of China
⁵⁵Suranaree University of Technology, University Avenue 111, Nakhon Ratchasima 30000, Thailand
⁵⁶Tsinghua University, Beijing 100084, People's Republic of China
^{57a}Turkish Accelerator Center Particle Factory Group, Istinye University, 34010 Istanbul, Turkey
^{57b}Near East University, Nicosia, North Cyprus, Mersin 10, Turkey
⁵⁸University of Chinese Academy of Sciences, Beijing 100049, People's Republic of China
⁵⁹University of Groningen, NL-9747 AA Groningen, The Netherlands
⁶⁰University of Hawaii, Honolulu, Hawaii 96822, USA
⁶¹University of Jinan, Jinan 250022, People's Republic of China
⁶²University of Manchester, Oxford Road, Manchester M13 9PL, United Kingdom
⁶³University of Muenster, Wilhelm-Klemm-Strasse 9, 48149 Muenster, Germany
⁶⁴University of Oxford, Keble Road, Oxford OX13RH, United Kingdom
⁶⁵University of Science and Technology Liaoning, Anshan 114051, People's Republic of China
⁶⁶University of Science and Technology of China, Hefei 230026, People's Republic of China
⁶⁷University of South China, Hengyang 421001, People's Republic of China
⁶⁸University of the Punjab, Lahore-54590, Pakistan
^{69a}University of Turin and INFN, University of Turin, I-10125 Turin, Italy
^{69b}University of Eastern Piedmont, I-15121 Alessandria, Italy
^{69c}INFN, I-10125, Turin, Italy
⁷⁰Uppsala University, Box 516, SE-75120 Uppsala, Sweden
⁷¹Wuhan University, Wuhan 430072, People's Republic of China
⁷²Xinyang Normal University, Xinyang 464000, People's Republic of China
⁷³Yunnan University, Kunming 650500, People's Republic of China
⁷⁴Zhejiang University, Hangzhou 310027, People's Republic of China
⁷⁵Zhengzhou University, Zhengzhou 450001, People's Republic of China

^aAlso at the Moscow Institute of Physics and Technology, Moscow 141700, Russia.

^bAlso at the Novosibirsk State University, Novosibirsk 630090, Russia.

^cAlso at the NRC "Kurchatov Institute," PNPI, 188300 Gatchina, Russia.

^dAlso at Goethe University Frankfurt, 60323 Frankfurt am Main, Germany.

^eAlso at Key Laboratory for Particle Physics, Astrophysics and Cosmology, Ministry of Education; Shanghai Key Laboratory for Particle Physics and Cosmology; Institute of Nuclear and Particle Physics, Shanghai 200240, People's Republic of China.

^fAlso at Key Laboratory of Nuclear Physics and Ion-beam Application (MOE) and Institute of Modern Physics, Fudan University, Shanghai 200443, People's Republic of China.

^gAlso at State Key Laboratory of Nuclear Physics and Technology, Peking University, Beijing 100871, People's Republic of China.

^hAlso at School of Physics and Electronics, Hunan University, Changsha 410082, China.

ⁱAlso at Guangdong Provincial Key Laboratory of Nuclear Science, Institute of Quantum Matter, South China Normal University, Guangzhou 510006, China.

^jAlso at Frontiers Science Center for Rare Isotopes, Lanzhou University, Lanzhou 730000, People's Republic of China.

^kAlso at Lanzhou Center for Theoretical Physics, Lanzhou University, Lanzhou 730000, People's Republic of China.

^lAlso at the Department of Mathematical Sciences, IBA, Karachi, Pakistan.

 (Received 9 August 2022; accepted 16 November 2022; published 5 December 2022)

We report a branching fraction measurement of the singly Cabibbo-suppressed decay $\Lambda_c^+ \rightarrow \Lambda K^+$ using a data sample collected with the BESIII detector at the BEPCII storage ring. The data span center-of-mass energies from 4.599 to 4.950 GeV and correspond to an integrated luminosity of 6.44 fb^{-1} . The branching fraction of $\Lambda_c^+ \rightarrow \Lambda K^+$ relative to that of the Cabibbo-favored decay $\Lambda_c^+ \rightarrow \Lambda \pi^+$ is measured to be $\mathcal{R} = \frac{\mathcal{B}(\Lambda_c^+ \rightarrow \Lambda K^+)}{\mathcal{B}(\Lambda_c^+ \rightarrow \Lambda \pi^+)} = (4.78 \pm 0.34 \pm 0.20)\%$. Combining with the world-average value of $\mathcal{B}(\Lambda_c^+ \rightarrow \Lambda \pi^+)$, we obtain $\mathcal{B}(\Lambda_c^+ \rightarrow \Lambda K^+) = (6.21 \pm 0.44 \pm 0.26 \pm 0.34) \times 10^{-4}$. Here the first uncertainties are statistical, the second systematic, and the third comes from the uncertainty of the $\Lambda_c^+ \rightarrow \Lambda \pi^+$ branching fraction. This result, which is more precise than previous measurements, does not agree with theoretical predictions, and suggests that nonfactorizable contributions have been underestimated in current models.

DOI: [10.1103/PhysRevD.106.L111101](https://doi.org/10.1103/PhysRevD.106.L111101)

Since its discovery, there has been continuous interest in understanding the nature of the Λ_c^+ charmed baryon [1]. Composed of three different quarks, the Λ_c^+ system is more complicated than the charmed-meson case and shows a different behavior in both lifetime and decays [2]. As the lowest-lying charmed baryon state, typical decays of the Λ_c^+ involve the weak interaction. Unlike for the case of charmed-meson decays where the factorizable contributions are dominant due to the large amount of emitted energy [3], the hadronic weak decays of the Λ_c^+ are neither color nor helicity suppressed [4], and are thus subject to sizable nonfactorizable contributions, such as W -exchange diagrams. This phenomenon is observed in recent experimental studies of the decays $\Lambda_c^+ \rightarrow \Sigma^0 \pi^+$, $\Lambda_c^+ \rightarrow \Sigma^+ \pi^0$ [5] and $\Lambda_c^+ \rightarrow \Xi^0 K^+$ [6], which indicate that nonfactorizable contributions are important.

To effectively describe the hadronic weak decay of the Λ_c^+ baryon, theoretical approaches such as current algebra [7], $SU(3)$ flavor symmetry [8,9] etc. are employed to calculate the decay rates. However, it is challenging to directly evaluate the nonfactorizable decay amplitudes in a model-independent manner, and so the theoretical predictions rely on phenomenological models. Experimentally, progress in the investigations of Λ_c^+ decay has been relatively slow due to the lack of experimental data in recent decades, especially for Cabibbo-suppressed decays whose branching fractions are usually smaller than 10^{-3} . Therefore, further precise measurements of the branching fractions of Λ_c^+ hadronic weak decays are eagerly sought in order to confront theory. Moreover, experimental measurements can also be taken as input to constrain these phenomenological models, as they quantify the nonfactorizable effects, and thus will help to improve our understanding of the dynamics of charmed baryons.

The singly Cabibbo-suppressed decay $\Lambda_c^+ \rightarrow \Lambda K^+$ was first studied by the Belle [10] and *BABAR* [11] collaborations more than 15 years ago. Belle measured the branching fraction of $\Lambda_c^+ \rightarrow \Lambda K^+$ relative to $\Lambda_c^+ \rightarrow \Lambda \pi^+$ to be $\mathcal{R} = \frac{\mathcal{B}(\Lambda_c^+ \rightarrow \Lambda K^+)}{\mathcal{B}(\Lambda_c^+ \rightarrow \Lambda \pi^+)} = (7.4 \pm 1.0 \pm 1.2)\%$, while *BABAR* reported $\mathcal{R} = (4.4 \pm 0.4 \pm 0.3)\%$. These two results differ from each other by around 2σ . Figure 1 shows the tree-level Feynman diagrams for $\Lambda_c^+ \rightarrow \Lambda K^+(\pi^+)$. The contribution from penguin diagrams are 6 orders of magnitude lower and are thus ignored here [12]. The external-emission diagram shown in Fig. 1(a) is factorizable and contributes $\sim(\tan \theta_c f_K/f_\pi)^2 = 7.6\%$ to the relative branching fraction $\frac{\mathcal{B}(\Lambda_c^+ \rightarrow \Lambda K^+)}{\mathcal{B}(\Lambda_c^+ \rightarrow \Lambda \pi^+)}$ (neglecting the mass difference between pion and kaon), where θ_c is the Cabibbo-mixing angle and $f_K(f_\pi)$ is the $K(\pi)$ decay constant. A more detailed calculation that takes into account the q^2 -dependent $\Lambda_c - \Lambda$ form factors and $K(\pi)$ mass difference gives the relative decay branching fraction from this factorizable diagram to be $\mathcal{R}_{\text{fac}} = (7.43 \pm 0.14)\%$ [13], where the uncertainty comes from knowledge of the form factors. References [8,14,15] have calculated the branching fraction of $\Lambda_c^+ \rightarrow \Lambda K^+$ including the nonfactorizable contributions of Figs. 1(b)–1(d), employing different approaches as summarized in Table I (note that the results from

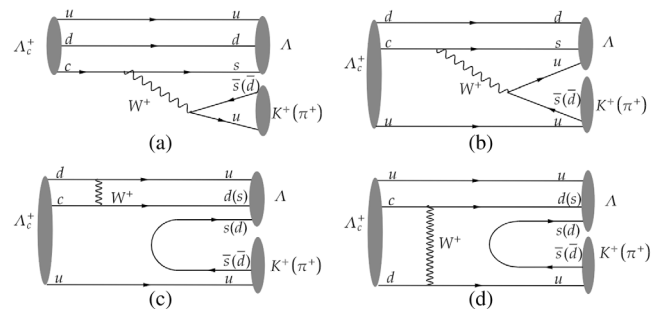


FIG. 1. The (a) external emission, (b) internal emission, and (c),(d) W -exchange Feynman diagrams for $\Lambda_c^+ \rightarrow \Lambda K^+$ and $\Lambda_c^+ \rightarrow \Lambda \pi^+$.

Published by the American Physical Society under the terms of the [Creative Commons Attribution 4.0 International license](https://creativecommons.org/licenses/by/4.0/). Further distribution of this work must maintain attribution to the author(s) and the published article's title, journal citation, and DOI. Funded by SCOAP³.

TABLE I. Theoretical predictions on the branching fraction of $\Lambda_c^+ \rightarrow \Lambda K^+$.

Theoretical predictions	$\mathcal{B}(\Lambda_c^+ \rightarrow \Lambda K^+) (\times 10^{-3})$
$SU(3)$ flavor symmetry [8]	1.4
Constituent quark model [14]	1.2
Current algebra [15]	1.06
Diquark picture [16]	0.18–0.39
$SU(3)$ flavor symmetry [17]	0.46 ± 0.09

Refs. [16,17] are not pure predictions and depend on fits to data).

In this paper, we report an improved measurement of the branching fraction of the singly Cabibbo-suppressed decay $\Lambda_c^+ \rightarrow \Lambda K^+$ (referred to as the signal mode) relative to the Cabibbo-favored decay $\Lambda_c^+ \rightarrow \Lambda \pi^+$ (referred to as the reference mode) using a single tag (ST) reconstruction method in $e^+e^- \rightarrow \Lambda_c^+ \bar{\Lambda}_c^-$ production. The Λ is reconstructed through the $p\pi^-$ decay. Throughout this paper, charge conjugation is always implied unless stated explicitly. The analysis is based on $(6.44 \pm 0.04) \text{ fb}^{-1}$ of e^+e^- annihilation data [18,19] collected at center-of-mass (c.m.) energies from 4.599 to 4.950 GeV [19,20] with the BESIII detector at the BEPCII storage ring.

The BESIII detector [21] records symmetric e^+e^- collision events provided by the BEPCII storage ring [22], which operates in the c.m. energy range from 2.0 to 4.95 GeV. BESIII has collected large data samples in this energy region [23]. The cylindrical core of the BESIII detector covers 93% of the full solid angle and consists of a helium-based multilayer drift chamber (MDC), a plastic scintillator time-of-flight system (TOF), and a CsI(Tl) electromagnetic calorimeter (EMC), which are all enclosed in a superconducting solenoidal magnet providing a 1.0 T magnetic field. The solenoid is supported by an octagonal flux-return yoke with resistive plate counter muon identification modules interleaved with steel. The charged-particle momentum resolution at 1 GeV/c is 0.5%, and the dE/dx resolution is 6% for electrons from Bhabha scattering. The EMC measures photon energies with a resolution of 2.5% (5%) at 1 GeV in the barrel (end-cap) region. The time resolution in the TOF barrel region is 68 ps, while that in the end-cap region is 110 ps. The end-cap TOF system was upgraded in 2015 using multigap resistive plate chamber technology, providing a time resolution of 60 ps [24].

A GEANT4 [25] based Monte Carlo (MC) simulation package, which includes the geometric description of the BESIII detector and its response, is used to determine the detection efficiency of signal events, optimize event-selection criteria, and estimate the backgrounds. The simulation models the beam-energy spread and initial-state radiation (ISR) in e^+e^- annihilations with the KKMC generator [26]. For “signal MC” samples, we generate $e^+e^- \rightarrow \Lambda_c^+ \bar{\Lambda}_c^-$ MC events with $\Lambda_c^+ \rightarrow \Lambda K^+$ and $\Lambda_c^+ \rightarrow \Lambda \pi^+$, while the $\bar{\Lambda}_c^-$ baryon decays inclusively. The

number of signal MC events which are generated at each c.m. energy corresponds to that of data. For the ISR simulation, the production cross section of $e^+e^- \rightarrow \Lambda_c^+ \bar{\Lambda}_c^-$ measured by BESIII is incorporated into the KKMC program, and the helicity angular distribution $\cos\theta_{\Lambda_c^+}$ in the pair-production process $e^+e^- \rightarrow \Lambda_c^+ \bar{\Lambda}_c^-$ are also taken into account. For the signal (reference) mode $\Lambda_c^+ \rightarrow \Lambda K^+$ ($\Lambda_c^+ \rightarrow \Lambda \pi^+$), the decay angular distributions are described with consideration of the decay asymmetry parameters ($\alpha = -0.84$) of the Λ_c^+ and Λ baryons ($\alpha_- = 0.732, \alpha_+ = -0.758$) [2,27]. To estimate the proportion of background events, MC samples including the production of $\Lambda_c^+ \bar{\Lambda}_c^-$ pairs, non- $\Lambda_c^+ \bar{\Lambda}_c^-$ events, $D\bar{D}$ pairs, ISR production of the J/ψ and $\psi(3686)$ states, and the continuum processes are also generated with KKMC [26,28]. The known decay modes of charmed hadrons are simulated with EVTGEN [29] with branching fractions taken from the Particle Data Group [30], and the remaining unknown decay modes are simulated with LUNDCHARM [31].

Charged tracks detected in the MDC are required to be within $|\cos\theta| < 0.93$, where θ is defined with respect to the z axis, which is the symmetry axis of the MDC. The Λ candidate is reconstructed from a pair of oppositely charged tracks, which are identified as proton and pion, respectively. Particle identification (PID) [32] for charged tracks combines measurements of the energy loss in the MDC (dE/dx) and the flight time in the TOF to evaluate the likelihoods $\mathcal{L}(h)$ ($h = p, K, \pi$) for each hadron h hypothesis. Tracks are identified as protons when the proton hypothesis satisfies the requirements $\mathcal{L}(p) > \mathcal{L}(\pi)$ and $\mathcal{L}(p) > \mathcal{L}(K)$, while the charged pion is required to satisfy $\mathcal{L}(\pi) > \mathcal{L}(K)$. Due to the relative long lifetime of Λ , the proton and pion candidates are further constrained to a common secondary decay vertex. To effectively separate the secondary vertex from the e^+e^- interaction point (IP), we require the decay length of the Λ to be twice larger than its uncertainty. The mass window for a Λ candidate is defined as $1.111 < M(p\pi^-) < 1.121 \text{ GeV}/c^2$.

For the signal mode (reference mode), a bachelor kaon (pion) candidate which does not originate from Λ decay is also required. Since the bachelor kaon (pion) track comes directly from the IP, stricter requirements on the track parameters are applied. The distance of the closest approach to the IP is required to be within 10 cm along the beam direction, and 1 cm in the plane perpendicular to the beam direction. PID is used to separate the signal mode (ΛK^+) from the reference mode ($\Lambda \pi^+$), i.e. the bachelor kaon (pion) candidate is required to satisfy $\mathcal{L}(K) > \mathcal{L}(\pi)$ [$\mathcal{L}(\pi) > \mathcal{L}(K)$].

The Λ and bachelor kaon (pion) candidates are combined to reconstruct the Λ_c^+ candidates. Two kinematic variables, the energy difference $\Delta E = E_{\Lambda_c^+} - E_{\text{beam}}$ and the beam-constrained mass $M_{\text{BC}} = \sqrt{E_{\text{beam}}^2/c^4 - |\vec{p}_{\Lambda_c^+}|^2/c^2}$ are used

to identify Λ_c^+ candidates. Here E_{beam} is the beam energy and $E_{\Lambda_c^+}$ and $\vec{p}_{\Lambda_c^+}$ are the measured energy and momentum of the Λ_c^+ candidate in the e^+e^- c.m. frame. When multiple Λ_c^+ candidates are found in one event, only the one with the minimum $|\Delta E|$ is retained for further analysis. A Λ_c^+ candidate is finally accepted if $-0.009 < \Delta E < 0.012$ GeV.

By investigating the MC background events with a generic event-type analysis tool, TOPOANA [33], we find that the main background in the $\Lambda_c^+ \rightarrow \Lambda K^+$ selection comes from $\Lambda_c^+ \rightarrow \Lambda e^+ \nu_e$ and $\Lambda_c^+ \rightarrow \Sigma^0 \pi^+$ decays. The background process $\Lambda_c^+ \rightarrow \Lambda e^+ \nu_e$ is rejected by requiring the deposited energy in the EMC divided by the momentum in the MDC (E/p) to be less than 0.9 for the kaon candidate. This requirement removes about 80% of background events, with a signal efficiency loss of about 2.7%, as indicated by MC simulation. To avoid losing too much signal efficiency, there is no requirement applied to suppress $\Sigma^0 \pi^+$ contamination. We find that the $\Lambda_c^+ \rightarrow \Sigma^0 \pi^+$ decay, as well as other irreducible Λ_c^+ decay backgrounds, contribute a smooth component in the M_{BC} distribution, which can be well simulated by MC events.

Figure 2 shows the M_{BC} distribution of the accepted candidates for $\Lambda_c^+ \rightarrow \Lambda \pi^+$ and $\Lambda_c^+ \rightarrow \Lambda K^+$ from the full dataset, where clear Λ_c^+ signals can be observed. To reduce the uncertainty of the $\Lambda_c^+ \rightarrow \Lambda K^+$ branching-fraction measurement, we measure the branching fraction of $\Lambda_c^+ \rightarrow \Lambda K^+$ relative to that of $\Lambda_c^+ \rightarrow \Lambda \pi^+$. A simultaneous fit is performed to the M_{BC} distributions for the datasets at each of the 13 c.m. energies, and the signal yield $N_i^{\Lambda K^+}$ for $\Lambda_c^+ \rightarrow \Lambda K^+$ events at the i th c.m. energy is further constrained by the relation $N_i^{\Lambda \pi^+} \frac{\epsilon_i^{\Lambda K^+}}{\epsilon_i^{\Lambda \pi^+}} \mathcal{R}$, where $\epsilon_i^{\Lambda K^+}$ ($\epsilon_i^{\Lambda \pi^+}$) is the detection efficiency for the signal (reference) mode, $N_i^{\Lambda \pi^+}$ is the signal yield for the reference mode at the i th c.m. energy, and $\mathcal{R} = \frac{\mathcal{B}(\Lambda_c^+ \rightarrow \Lambda K^+)}{\mathcal{B}(\Lambda_c^+ \rightarrow \Lambda \pi^+)}$ is the relative branching fraction. The detection efficiencies for the signal and reference modes are estimated by analyzing signal MC events with the same

procedure as for the data analysis, and are listed in Table II. Due to the effects of ISR, the detection efficiencies for events at $\sqrt{s} > 4.7$ GeV are slightly lower (between 23% and 29%), but the relative efficiency between the signal mode and the reference mode at the same c.m. energy is quite stable. Thus, these samples, each of which has a low signal yield, are combined into a merged dataset.

The probability-density functions are constructed with the sum of signal and background components at each c.m. energy. The signal components are modeled with the corresponding MC simulated shapes convolved with Gaussian functions, which account for the resolution difference between data and MC simulation. Here, the standard deviations of the smearing Gaussian resolution function for $\Lambda_c^+ \rightarrow \Lambda K^+$ events are constrained to the ones obtained from the fits to $\Lambda_c^+ \rightarrow \Lambda \pi^+$ events to improve precision, and the mean values are left as free parameters. The background components are described by ARGUS functions [34] with the truncation parameters fixed to E_{beam} at each c.m. energy. The simultaneous fit gives

$$\mathcal{R} = \frac{\mathcal{B}(\Lambda_c^+ \rightarrow \Lambda K^+)}{\mathcal{B}(\Lambda_c^+ \rightarrow \Lambda \pi^+)} = (4.78 \pm 0.34)\%, \quad (1)$$

where the uncertainty is statistical only. The fit results for the sum of all datasets are shown in Fig. 2, where the background curve is the sum of a series of ARGUS functions with a floating end point (E_{beam}) and showing a complicated distribution. The corresponding results at each individual c.m. energy are listed in the Appendix.

The main sources of systematic uncertainty on the \mathcal{R} measurement are related to tracking, PID, E/p requirement, signal shape, and background shape. It should be noted that many systematic sources, such as those associated with the total number of $\Lambda_c^+ \bar{\Lambda}_c^-$ events, Λ reconstruction, etc., are common to the signal and reference modes and thus cancel in the \mathcal{R} measurement. In the following, we only discuss the uncorrelated sources for the signal and the reference modes.

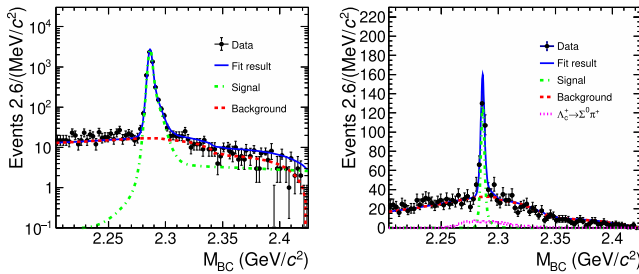


FIG. 2. A simultaneous fit to the M_{BC} distributions of the candidates for (left) $\Lambda_c^+ \rightarrow \Lambda \pi^+$ and (right) $\Lambda_c^+ \rightarrow \Lambda K^+$. The points with error bars are the full data, the blue solid curves are the sum of fit results at each c.m. energy, the green dot-dashed curves are the signal components, the red dashed curves are the background components, and the magenta dotted curve in the right panel is the normalized $\Sigma^0 \pi^+$ background.

TABLE II. The integrated luminosity (\mathcal{L}) of dataset, signal yield (N) for $\Lambda \pi^+$ mode from the fit, and the detection efficiencies (ϵ in percentage) for $\Lambda_c^+ \rightarrow \Lambda K^+$ and $\Lambda_c^+ \rightarrow \Lambda \pi^+$ modes, respectively at each c.m. energy. Here the uncertainties are statistical only.

\sqrt{s} (GeV)	\mathcal{L} (pb $^{-1}$)	$N(\Lambda \pi^+)$	$\epsilon(\Lambda \pi^+)$	$\epsilon(\Lambda K^+)$
4.5999	586.9 ± 3.9	539.8 ± 22.5	37.9 ± 0.2	36.6 ± 0.3
4.6118	103.8 ± 0.6	92.1 ± 9.4	34.4 ± 0.2	33.1 ± 0.2
4.6277	521.5 ± 2.8	502.4 ± 21.4	33.4 ± 0.2	32.6 ± 0.2
4.6409	552.4 ± 3.0	507.8 ± 21.6	33.7 ± 0.2	31.6 ± 0.2
4.6613	529.6 ± 2.9	491.4 ± 21.1	32.5 ± 0.2	30.9 ± 0.2
4.6812	1669.3 ± 9.0	1470.8 ± 36.3	31.4 ± 0.2	29.3 ± 0.2
4.6984	536.5 ± 2.9	374.7 ± 18.1	30.2 ± 0.2	28.6 ± 0.2
> 4.700	1940.1 ± 11.6	896.3 ± 27.8	24.9–29.5	23.6–28.5

The tracking efficiency of the bachelor K and π in the signal and reference modes is not exactly the same due to different momentum distributions, and this leads to an uncertainty in the measurement. A control sample of $e^+e^- \rightarrow K^+K^-\pi^+\pi^-$ is used to study the tracking efficiency of both kaons and pions [35], and the tracking uncertainties $\delta(p_T)$ for various transverse momentum intervals are obtained by comparing the efficiency difference between data and MC simulation. By assigning each event from the signal MC samples with a corresponding weight $[1 + \delta(p_T)]$ for both the signal and reference modes, we reevaluate the detection efficiencies and find the relative branching-fraction measurement changes by 1.1%, which is the systematic uncertainty due to tracking efficiency.

The PID efficiencies for charged kaons and pions are studied with control samples of $D_s^+ \rightarrow K^+K^-\pi^+$, $D^0 \rightarrow K^-\pi^+$, $D^0 \rightarrow K^-\pi^+\pi^+\pi^-$ decays [35], and the efficiency difference $\delta(p)$ between data and MC simulation for different kaon and pion momentum intervals is obtained. A method similar to the one adopted for tracking is applied to assign a systematic uncertainty of 1.2% associated with the PID efficiencies for both the signal and reference modes.

The E/p requirement introduces a minor efficiency loss for kaons. The associated systematic uncertainty is assigned to be 0.4% from measuring the efficiency difference between data and MC simulation in a control sample of $\Lambda_c^+ \rightarrow pK^-\pi^+$ decays.

The systematic uncertainty due to the choice of signal shape is studied by fitting the data with an alternative shape, with free parameters for the smearing Gaussian function of $\Lambda_c^+ \rightarrow \Lambda K^+$ mode in the fit. The change in the signal yield, 0.9%, is taken as the systematic uncertainty.

To estimate the systematic uncertainty associated with the background shape, we parametrize the background component with an ARGUS function plus the $\Lambda_c^+ \bar{\Lambda}_c^-$ inclusive MC shape (accounting for possible unknown Λ_c^+ decays), or a shape derived from wrong-sign data events. The largest deviation with respect to the nominal fit result, 2.4%, is taken as the systematic uncertainty from this source.

The possible systematic bias due to the value of the $\Lambda_c^+ \rightarrow \Lambda K^+$ decay-asymmetry parameters is studied by considering a range of theoretical predictions for these parameters [8,14] as well as a result from the Belle collaboration [36]. The $\Lambda_c^+ \rightarrow \Lambda K^+$ MC samples are resimulated based on these different values and the detection efficiencies are recalculated. The largest deviation with respect to the baseline fit result, 3%, is assigned as the systematic uncertainty.

Assuming all these sources are independent, the total systematic uncertainty is calculated to be 4.3% by adding each contribution in quadrature.

In summary, based on an e^+e^- annihilation data sample of $(6.44 \pm 0.04) \text{ fb}^{-1}$ collected at c.m. energies from $\sqrt{s} = 4.599$ to 4.950 GeV with the BESIII detector at the BEPCII storage ring, a study of the singly

Cabibbo-suppressed decay $\Lambda_c^+ \rightarrow \Lambda K^+$ and the Cabibbo-favored decay $\Lambda_c^+ \rightarrow \Lambda \pi^+$ is performed by using a ST method. The relative decay branching fraction is measured to be $\mathcal{R} = (4.78 \pm 0.34 \pm 0.20)\%$, where the first uncertainty is statistical and the second systematic. Our result is consistent with the measurements performed by the Belle [10] and BABAR [11] collaborations within uncertainties, but closer to that of BABAR. It improves the precision of the PDG average value (0.047 ± 0.009) [2] by a factor of more than 2 and disfavors theoretical predictions [8,14,15]. By taking the branching fraction of $\mathcal{B}(\Lambda_c^+ \rightarrow \Lambda \pi^+) = (1.30 \pm 0.07)\%$ as input [2], we determine $\mathcal{B}(\Lambda_c^+ \rightarrow \Lambda K^+) = (6.21 \pm 0.44 \pm 0.26 \pm 0.34) \times 10^{-4}$.

The measured branching fraction of $\Lambda_c^+ \rightarrow \Lambda K^+$ is significantly lower ($\sim 40\%$) than the predictions based on the $SU(3)$ flavor symmetry, constituent quark model, or current algebra [15] listed in Table I. As the pure factorizable contribution is reliably calculated for the relative branching fraction [$\mathcal{R}_{\text{fac}} = (7.43 \pm 0.14)\%$ [13]], we determine the contribution from the nonfactorizable effect to be $\mathcal{R}_{\text{non-fac}} = \mathcal{R} - \mathcal{R}_{\text{fac}} = -(2.65 \pm 0.42)\%$, which is negative and has a size comparable to the factorizable contribution. This indicates that the nonfactorizable contributions in Λ_c^+ decay are important and have been significantly underestimated in current theoretical models.

It is illustrative to compare our result with analogous ratios measured in different systems. The ratio of singly Cabibbo-suppressed to Cabibbo-favored decays of Λ_b baryons has been measured to be $\frac{\mathcal{B}(\Lambda_b \rightarrow \Lambda_c^+ K^-)}{\mathcal{B}(\Lambda_b \rightarrow \Lambda_c^+ \pi^-)} = (7.31 \pm 0.16 \pm 0.16)\%$ by the LHCb collaboration [37], which is consistent with the naive expectation $(\tan \theta_c f_K / f_\pi)^2$, and so significantly different for the case with Λ_c baryons. A comparison with $\frac{\mathcal{B}(\Lambda_c^+ \rightarrow p K^+ \pi^-)}{\mathcal{B}(\Lambda_c^+ \rightarrow p K^-\pi^+)} = (0.82 \pm 0.12) \tan^4 \theta_c$ measured by Belle [38] shows that the nonfactorizable contribution in Λ_c^+ singly Cabibbo-suppressed decay seems to have a more prominent effect. Compared with $\frac{\mathcal{B}(D^0 \rightarrow K^+ \pi^-)}{\mathcal{B}(D^0 \rightarrow K^-\pi^+)} = (1.24 \pm 0.05) \tan^4 \theta_c$ measured by LHCb [39] or $\sqrt{\frac{\mathcal{B}(D^+ \rightarrow K^+ \pi^+ \pi^-) \mathcal{B}(D_s^+ \rightarrow K^+ K^+ \pi^-)}{\mathcal{B}(D^+ \rightarrow K^-\pi^+ \pi^+) \mathcal{B}(D_s^+ \rightarrow K^+ K^-\pi^+)}} = (1.25 \pm 0.08) \tan^4 \theta_c$ measured by Belle [40], our measurement indicates that the $SU(3)$ flavor-symmetry breaking in the charmed baryon system is more significant than that in the charmed meson case.

The BESIII collaboration thanks the staff of BEPCII and the IHEP computing center for their strong support. This work is supported in part by National Key R&D Program of China under Contracts No. 2020YFA0406400 and No. 2020YFA0406300; National Natural Science Foundation of China (NSFC) under Contracts No. 11635010, No. 11735014, No. 11835012, No. 11935015, No. 11935016, No. 11935018, No. 11961141012, No. 12022510, No. 12025502, No. 12035009, No. 12035013, No. 12192260, No. 12192261, No. 12192262, No. 12192263, No. 12192264, and No. 12192265; the Chinese Academy of Sciences

(CAS) Large-Scale Scientific Facility Program; Joint Large-Scale Scientific Facility Funds of the NSFC and CAS under Contract No. U1832207; 100 Talents Program of CAS; Project No. ZR2022JQ02 supported by Shandong Provincial Natural Science Foundation; The Institute of Nuclear and Particle Physics (INPAC) and Shanghai Key Laboratory for Particle Physics and Cosmology; ERC under Contract No. 758462; European Union's Horizon 2020 research and innovation program under Marie Skłodowska-Curie Grant Agreement under Contract No. 894790; German Research Foundation DFG under Contracts No. 443159800, Collaborative Research Center CRC 1044, GRK 2149; Istituto Nazionale di Fisica Nucleare, Italy; Ministry of Development of Turkey under Contract No. DPT2006K-120470; National Science and Technology fund; National Science Research and Innovation Fund

(NSRF) via the Program Management Unit for Human Resources & Institutional Development, Research and Innovation under Contract No. B16F640076; STFC (United Kingdom); Suranaree University of Technology (SUT), Thailand Science Research and Innovation (TSRI), and National Science Research and Innovation Fund (NSRF) under Contract No. 160355; The Royal Society, UK, under Contracts No. DH140054 and No. DH160214; The Swedish Research Council; U.S. Department of Energy under Contract No. DE-FG02-05ER41374.

APPENDIX: SIMULTANEOUS FIT PLOTS FOR THIRTEEN C.M. ENERGY

Figure 3 shows the fit to the M_{BC} distribution at each c.m. energy.

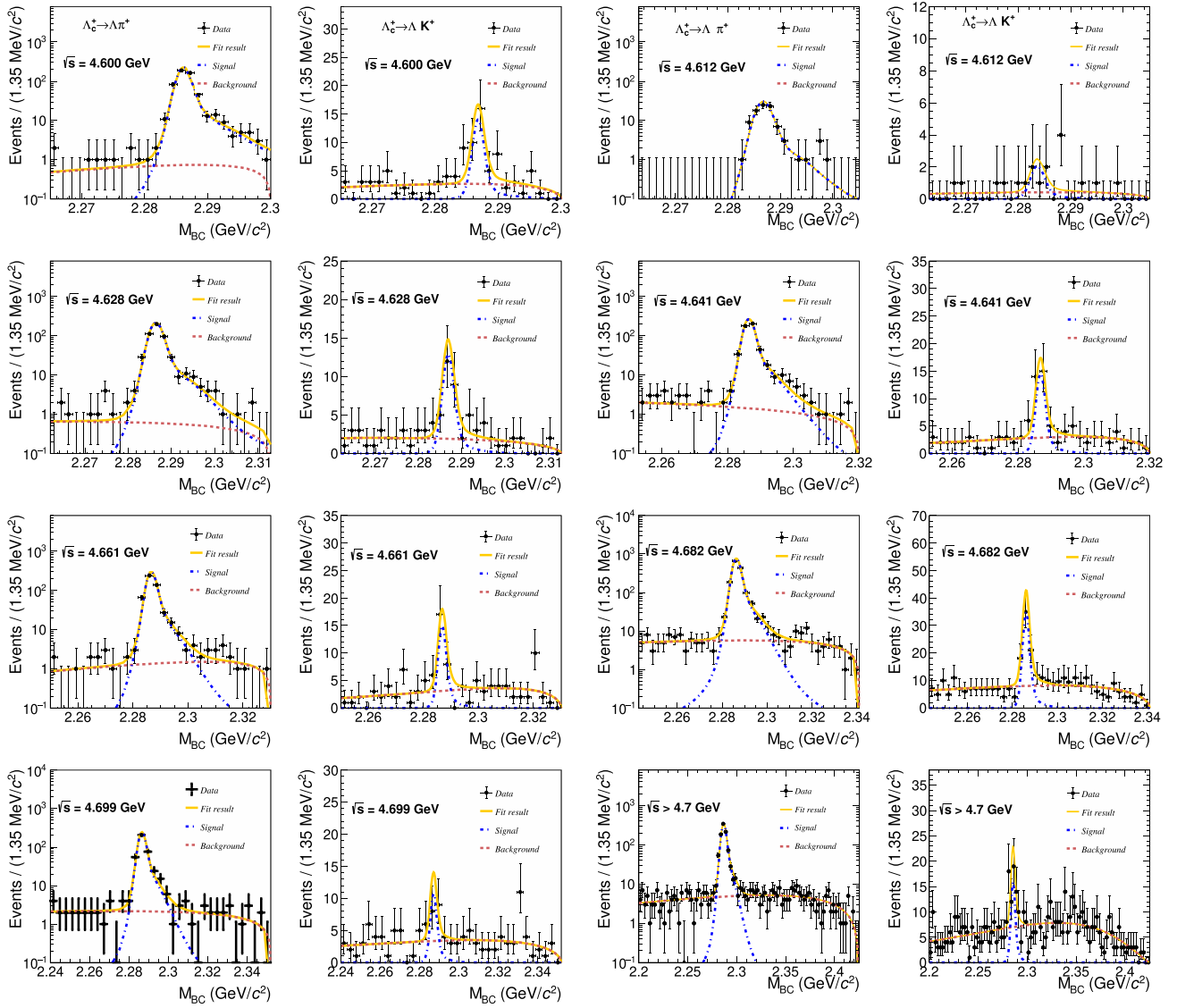


FIG. 3. Simultaneous fit result to the M_{BC} distributions of the $\Lambda_c^+ \rightarrow \Lambda\pi^+$ (left) and $\Lambda_c^+ \rightarrow \Lambda K^+$ (right) candidates at various c.m. energy points. The points with error bars are data, the orange solid curves represent the fit results, the blue dot-dashed curves represent the Λ_c^+ signal, and the brown dashed curves represent the background components.

- [1] H. Y. Cheng, *Int. J. Mod. Phys. A* **24**, 593 (2009); *Front. Phys.* **10**, 101406 (2015); *Chin. J. Phys.* **78**, 324 (2022).
- [2] R. L. Workman *et al.* (Particle Data Group), *Prog. Theor. Exp. Phys.* **2022**, 083C01 (2022).
- [3] M. Bauer, B. Stech, and M. Wirbel, *Z. Phys. C* **34**, 103 (1987); Q. P. Xu and A. N. Kamal, *Phys. Rev. D* **46**, 270 (1992).
- [4] H. Y. Cheng, *Z. Phys. C* **29**, 127 (1985).
- [5] M. Ablikim *et al.* (BESIII Collaboration), *Phys. Rev. Lett.* **116**, 052001 (2016).
- [6] M. Ablikim *et al.* (BESIII Collaboration), *Phys. Lett. B* **783**, 200 (2018).
- [7] H. Y. Cheng and B. Tseng, *Phys. Rev. D* **48**, 4188 (1993); K. K. Sharma and R. C. Verma, *Eur. Phys. J. C* **7**, 217 (1999).
- [8] K. K. Sharma and R. C. Verma, *Phys. Rev. D* **55**, 7067 (1997).
- [9] C. D. Lü, W. Wang, and F. S. Yu, *Phys. Rev. D* **93**, 056008 (2016).
- [10] K. Abe *et al.* (Belle Collaboration), *Phys. Lett. B* **524**, 33 (2002).
- [11] B. Aubert *et al.* (BABAR Collaboration), *Phys. Rev. D* **75**, 052002 (2007).
- [12] H. N. Li, C. D. Lü, and F. S. Yu, *Phys. Rev. D* **86**, 036012 (2012).
- [13] S. S. Bao, [arXiv:2208.00557](https://arxiv.org/abs/2208.00557).
- [14] T. Uppal, R. C. Verma, and M. P. Khanna, *Phys. Rev. D* **49**, 3417 (1994).
- [15] H. Y. Cheng, X. W. Kang, and F. R. Xu, *Phys. Rev. D* **97**, 074028 (2018).
- [16] S. L. Chen, X. H. Guo, X. Q. Li, and G. L. Wang, *Commun. Theor. Phys.* **40**, 563 (2003).
- [17] C. Q. Geng, Y. K. Hsiao, and Y. H. Lin, *Phys. Lett. B* **776**, 265 (2018).
- [18] M. Ablikim *et al.* (BESIII Collaboration), *Chin. Phys. C* **39**, 093001 (2015).
- [19] M. Ablikim *et al.* (BESIII Collaboration), *Chin. Phys. C* **46**, 113003 (2022).
- [20] M. Ablikim *et al.* (BESIII Collaboration), *Chin. Phys. C* **40**, 063001 (2016).
- [21] M. Ablikim *et al.* (BESIII Collaboration), *Nucl. Instrum. Methods Phys. Res., Sect. A* **614**, 345 (2010).
- [22] C. H. Yu *et al.*, *Proceedings of the IPAC2016, Busan, Korea* (JACoW, Geneva, Switzerland, 2016).
- [23] M. Ablikim *et al.* (BESIII Collaboration), *Chin. Phys. C* **44**, 040001 (2020).
- [24] X. Li *et al.*, *Nucl. Instrum. Methods Phys. Res., Sect. A* **953**, 163053 (2020).
- [25] S. Agostinelli *et al.* (GEANT4 Collaboration), *Nucl. Instrum. Methods Phys. Res., Sect. A* **506**, 250 (2003).
- [26] S. Jadach, B. F. L. Ward, and Z. Was, *Phys. Rev. D* **63**, 113009 (2001).
- [27] H. Chen and R. G. Ping, *Phys. Rev. D* **99**, 114027 (2019).
- [28] S. Jadach, B. F. L. Ward, and Z. Was, *Comput. Phys. Commun.* **130**, 260 (2000).
- [29] D. J. Lange, *Nucl. Instrum. Methods Phys. Res., Sect. A* **462**, 152 (2001).
- [30] M. Tanabashi *et al.*, *Phys. Rev. D* **98**, 030001 (2018).
- [31] J. C. Chen, G. S. Huang, X. R. Qi, D. H. Zhang, and Y. S. Zhu, *Phys. Rev. D* **62**, 034003 (2000); R. L. Yang, R. G. Ping, and H. Chen, *Chin. Phys. Lett.* **31**, 061301 (2014).
- [32] M. K. He, J. Hu, B. Huang, G. Qin, S. Sun, J. Zhang, and Y. Zheng, *Proc. Sci., ACAT2007* (**2007**) 038.
- [33] X. Y. Zhou, S. X. Du, G. Li, and C. P. Shen, *Comput. Phys. Commun.* **258**, 107540 (2021).
- [34] H. Albrecht *et al.*, *Phys. Lett. B* **241**, 278 (1990).
- [35] M. Ablikim *et al.* (BESIII Collaboration), *Phys. Rev. D* **99**, 112005 (2019); *J. High Energy Phys.* **08** (2022) 196.
- [36] K. Abe *et al.* (Belle Collaboration), [arXiv:2208.08695](https://arxiv.org/abs/2208.08695).
- [37] R. Aaij *et al.* (LHCb Collaboration), *Phys. Rev. D* **89**, 032001 (2014).
- [38] S. B. Yang *et al.* (Belle Collaboration), *Phys. Rev. Lett.* **117**, 011801 (2016).
- [39] R. Aaij *et al.* (LHCb Collaboration), *Phys. Rev. Lett.* **110**, 101802 (2013).
- [40] B. R. Ko *et al.* (Belle Collaboration), *Phys. Rev. Lett.* **102**, 221802 (2009).